

See discussions, stats, and author profiles for this publication at: <https://www.researchgate.net/publication/273952521>

Protein Functionalized Carbon Nanotubes-based Smart Lab-on-a-Chip

ARTICLE in ACS APPLIED MATERIALS & INTERFACES · FEBRUARY 2015

Impact Factor: 6.72 · DOI: 10.1021/am509002h · Source: PubMed

CITATIONS

3

READS

124

7 AUTHORS, INCLUDING:



[Pratima R Solanki](#)

National Physical Laboratory - India

111 PUBLICATIONS 2,434 CITATIONS

[SEE PROFILE](#)



[Ved Varun Agrawal](#)

National Physical Laboratory - India

54 PUBLICATIONS 775 CITATIONS

[SEE PROFILE](#)



[Renu John](#)

Indian Institute of Technology Hyderabad

46 PUBLICATIONS 760 CITATIONS

[SEE PROFILE](#)



[Bansi Malhotra](#)

Delhi Technological University

327 PUBLICATIONS 9,405 CITATIONS

[SEE PROFILE](#)

Protein Functionalized Carbon Nanotubes-based Smart Lab-on-a-Chip

Md. Azahar Ali,^{†,‡} Pratima R. Solanki,[§] Saurabh Srivastava,^{†,||} Samer Singh,[§] Ved V. Agrawal,[†] Renu John,[‡] and Bansi D. Malhotra^{*,||}

[†]Biomedical Instrumentation Section, Materials Physics & Engineering Division, CSIR-National Physical Laboratory, Dr. K. S. Krishnan Marg, New Delhi 110012, India

[‡]Department of Biomedical Engineering, Indian Institute of Technology Hyderabad, Ordnance Factory Estate, Yedumailaram, Hyderabad, Andhra Pradesh 502205, India

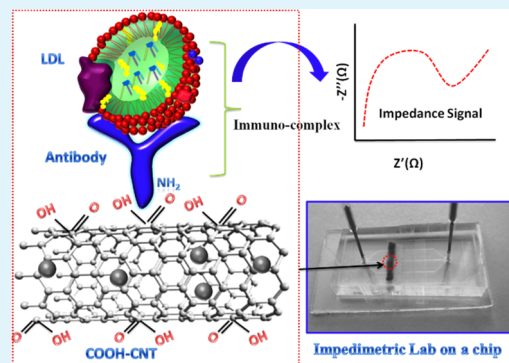
[§]Special Centre for Nano Sciences, Jawaharlal Nehru University, New Delhi 110067, India

^{||}Department of Biotechnology, Delhi Technological University, Main Bawana Road, Delhi 110042, India

Supporting Information

ABSTRACT: A label-free impedimetric lab on a chip (*i*LOC) is fabricated using protein (bovine serum albumin) and antiapolipoprotein B functionalized carbon nanotubes–nickel oxide (CNT–NiO) nanocomposite for low-density lipoprotein (LDL) detection. The antiapolipoprotein B (AAB) functionalized CNT–NiO microfluidic electrode is assembled with polydimethylsiloxane rectangular microchannels (cross section: 100 × 100 μm). Cytotoxicity of the synthesized CNTs, NiO nanoparticles, and CNT–NiO nanocomposite has been investigated in the presence of lung epithelial cancer A549 cell line using MTT assay. The CNT–NiO nanocomposite shows higher cell viability at a concentration of 6.5 $\mu\text{g}/\text{mL}$ compared to those using individual CNTs. The cell viability and proliferation studies reveal that the toxicity increases with increasing CNTs concentration. The X-ray photoelectron spectroscopy studies have been used to quantify the functional groups present on the CNT–NiO electrode surface before and after proteins functionalization. The binding kinetic and electrochemical activities of CNT–NiO based *i*LOC have been conducted using chronocoulometry and impedance spectroscopic techniques. This *i*LOC shows excellent sensitivity of 5.37 k Ω (mg/dL)⁻¹ and a low detection limit of 0.63 mg/dL in a wide concentration range (5–120 mg/dL) of LDL. The binding kinetics of antigen–antibody interaction of LDL molecules reveal a high association rate constant ($8.13 \text{ M}^{-1} \text{ s}^{-1}$). Thus, this smart nanocomposite (CNT–NiO) based *i*LOC has improved stability and reproducibility and has implications toward in vivo diagnostics.

KEYWORDS: *label-free immunosensor, lab-on-a-chip, impedance, cytotoxicity, low density lipoprotein, antiapolipoprotein B*



1. INTRODUCTION

The unique physical, chemical, and electronic properties of nanomaterials have been extensively explored for application in biomedical diagnostics including lab on a chip (LOC), biosensors, implantable medical devices (e.g. *in situ* monitoring) and bioimaging.^{1–3} Low-dimensional LOC, field-effect transistor-based biosensors, and bioelectronic devices based on carbon nanotubes (CNTs), graphene, and metal oxide/silicon nanowires have exceptional merits for point-of-care diagnostics and prognosis.^{4–6} Sharf et al. have utilized CNTs for development of field effect transistor-based biosensor to obtain the improved bioelectronic interface.⁷ The high conductivity, mechanical strength, and tunable functionality in conjugation with biomolecules, and electrochemical and good tribological characteristics of CNTs make it the promising candidate for fabrication of an ultrasensitive LOC for biomolecules

detection.^{8–10} Napier et al. have reported the electrochemical oxidation of DNA wrapped CNTs.⁹

The electrochemical properties of the CNTs can perhaps be enhanced by incorporating metal oxides nanoparticles such as nickel oxide, manganese oxide, and so on.¹¹ Ali et al. reported dispersion of CNTs in the presence of nickel oxide to obtain an efficient microfluidic biosensor for esterified cholesterol detection.¹² The nanostructured nickel oxide (nNiO) provides large surface-to-volume ratio, high electrocatalytic behavior, and biocompatibility and does not degrade on exposure to protein, enzyme, smRNA or DNA, antibody, and so on.¹³ The nNiO provides high isoelectric point (IEP ~ 10.8) that can be helpful for the immobilization of an antibody (IEP ~ 4.5) via

Received: December 21, 2014

Accepted: February 26, 2015

electrostatic interactions or attachment with other nanomaterials like CNTs that have a negative electrokinetic surface potential.¹⁴ The nNiO can be used to obtain enhanced electrochemical characteristics in the presence of mediator or redox probe due to bulk conduction, tunneling, and enhanced surface scattering of electrons arising due to high density of electronic states. It has been reported that CNTs perhaps provide an electronic path for transport of the charge carriers in the electrode surface from electrolyte solution. Besides this, the integrated LOC possesses remarkable characteristics over the conventional biosensor devices due to reduced consumption of reagents/samples, power consumption and compact size.^{15,16} The electrochemical impedance change in electrode interface can be directly related to the concentration of bound target.¹⁷ The high surface-to-volume ratio of electrochemical LOC has been found to result in shorter assay times as well as label-free detection of specific biomolecules. The integrated LOC may perhaps be utilized for multiplex analysis of biorecognition events.¹⁸ On the basis of label-free detection, several detection strategies have been implemented for highly effective signal transduction of the biorecognition events via microfluidic platforms. Ali et al. have fabricated an immunosensor based on surface plasmon resonance (SPR) and electrochemical detection system using CdS quantum dots for monitoring LDL molecules.¹⁹ This immunosensor shows the sensitivity of $98.5 \Omega/(mg/dl)/cm^2$ and limit of detection is found to be as 16.03 mg/dl. The kinetics of antibody–antigen interactions of LDL molecules and their detection have been investigated using self-assembled monolayer of 4-aminothiophenol by Matharu et al.²⁰ Thus, a higher sensitive and miniaturized device for lipid molecules (low density lipoprotein, triglycerides, etc.) quantification is currently a major concern for point-of-care (POC) diagnostics.

CNTs have recently been used for development of biosensors/LOC, drug delivery systems, in vivo and in vitro biodistribution, and toxicity effect.^{21–23} CNTs coupled with a metal oxide can play an important role for multimodal bioimaging.⁸ However, the biocompatibility and cytotoxicity effect of CNTs are currently major limitations for the development of nanomaterials-based in vivo diagnostics devices. The toxicity associated with CNTs when they come in direct contact with body fluid has remained a cause of concern for biological applications.^{24–26} At the molecular level, it is important to understand the nature of interaction between a biosystem with a nanostructured material including CNTs. Ryoo et al. have described the mammalian cellular (NIH-3T3 fibroblast cells) response in the presence of CNTs/graphene.²⁷ It has been found that these nanomaterials show good performance for bioapplication including in situ monitoring of biomolecules, especially for implantable devices without inducing remarkable deleterious effects. Davoren et al. have investigated the in vitro cell viability of single walled carbon nanotubes on human A549 lung cells to evaluate the metabolic, lysosomal and mitochondrial activity.²⁸ Mooney et al. have tracked the intracellular movement of CNTs through the cytoplasm to a nuclear location of human mesenchymal stem cells and investigated the effects on cellular metabolic activity, proliferation and differentiation.²⁹ However, the cytotoxicity effect of metal oxide integrated CNTs hybrid nanomaterial is still unexplored for application to POC devices. Thus, there is urgent requirement to conduct a systematic investigation relating to toxicity of the hybrid nanomaterials that may be in contact with human cells for in vivo and in situ measurements,

such as in cell-based biosensors, LOC or implantable devices for biomolecule detection.

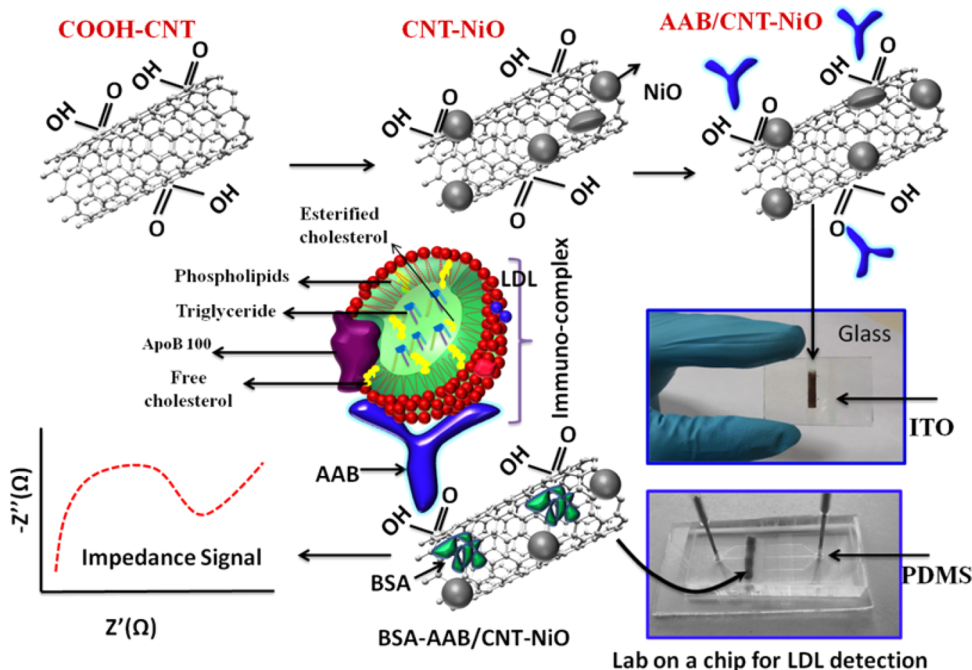
Estimation of low-density lipoprotein (LDL) cholesterol in human serum is urgently required via POC diagnostics.³⁰ Lipoproteins are known to play a vital role toward the transport of cholesterol in the bloodstream and are catabolized in the liver and kidneys, and in peripheral tissues via receptor-mediated endocytosis mechanisms. These lipoproteins are mainly synthesized in the liver and intestines, and are assembled at the cell membranes from cellular lipids and exogenous lipoproteins or apolipoproteins. They can be categorized by the electrophoretic mobility on agarose gels into pre-13, and 13 lipoproteins, corresponding to LDL, very-low-density lipoprotein, intermediate-density lipoprotein, and high-density lipoprotein, respectively. During cholesterol transportation, the interaction of apolipoprotein with sulfated glycosaminoglycans results in cholesterol accumulation in the arterial walls. This may cause plaque formation through arteries walls and make them less flexible, causing various heart and vascular diseases, such as atherosclerosis, and accompanying immune-inflammatory response.³¹ Nuclear magnetic resonance spectroscopy, ultracentrifugation, gel filtration, electrophoresis, Friedewald equation, and affinity chromatography are the conventional techniques currently used to estimate concentration of LDL molecules.³⁰ However, for general clinical use, these methods are expensive, time-consuming, and necessitate invention of alternative strategies. Apolipoprotein B can play an important role in receptor recognition via antigen–antibody interactions.

In this study, we demonstrate the fabrication of an impedimetric lab on a chip (iLOC) for label-free detection of LDL molecules. In this iLOC, the immunoelectrode has been fabricated using antiapolipoprotein B (AAB) and bovine serum albumin (BSA) functionalized carbon nanotubes-nickel oxide (CNT–NiO) nanocomposite deposited onto indium–tin oxide (ITO) substrate. The proteins conjugated CNT–NiO electrode has been characterized and quantified using spectroscopic and microscopic techniques. In addition, the cytotoxicity effect of NiO nanoparticles, CNTs, and CNT–NiO composite in the presence of human lung epithelial cancer cell (A549) using MTT assay has been investigated.

2. EXPERIMENTAL SECTION

2.1. Chemicals. The SU8–100 negative photoresist and Shipley 1811 positive photoresist for polydimethylsiloxane (PDMS) microchannels and ITO electrode fabrication, respectively, are procured from Microchem (Newton, MA). The $Ni(NO_3)_2$ (nickel nitrate) and KOH (potassium hydroxide) have been procured from Sigma-Aldrich (St. Louis, MO). LDL antiapolipoprotein B-100 (AAB), *N*-hydroxysuccinimide (NHS), *N*-ethyl-N-(3-(dimethylamino)propyl carbodiimide) (EDC) and bovine serum albumin (BSA) are purchased from Sigma-Aldrich (St. Louis, MO). Five milligrams (5 mg) of lyophilized LDL powder is used to dissolve in 1 mL of deionized water with 150 mM NaCl of pH 7.4 and 0.01% ethylene diaminetetra acetic acid. Then, 50 mM phosphate buffer saline (PBS) of pH 7.4 is used to prepare the BSA (2 mg/mL) and AAB (1 mg/mL) solutions containing 150 mM NaCl. Deionized water has been obtained from the Millipore water purification system.

2.1. Fabrication of LOC. Details of soft lithographic technique for PDMS microchannels and ITO electrode fabrication have been reported earlier.³² We carried out a slight modification in PDMS microchannels and ITO electrode to decrease the channel size. In brief, the soft lithographically has been utilized to fabricate the PDMS microchannels having height, length, and width of 100 μm , 2 cm, and 100 μm , respectively. On the other hand, the indium tin oxide (ITO)

Scheme 1. Schematic Representation of the Lab-on-a-Chip Fabrication For LDL Detection

electrode on glass substrate (size; $2\text{ mm} \times 2.6\text{ cm}$) has been fabricated using photolithographic technique followed by wet chemical etching as shown in Figure S1 (Supporting Information). Prior to use, the ITO is cleaned with acetone and methanol. A small amount of positive photoresist (Shipley 1811) is coated onto ITO substrate and allowed to spin at 3000 rpm for 20 s. The photoresist/ITO substrate is soft baked using a hot plate for 1 min to remove the solvent. The UV radiation is used to expose this photosensitive substrate followed by an optical mask. After UV exposure, the photoresist/ITO substrate is developed using a developer solution for 10 s. The developed substrate is then dipped into the ITO etchant (zinc dust + HCl solution 15%) to etch the ITO on glass substrate from the exposed region. The remaining photoresist on ITO is washed out by acetone. This ITO electrode on glass is again cleaned with acetone via sonication (15 min) and with deionized water several times. These clean ITO electrodes are hydrolyzed using the mixture of $\text{H}_2\text{O}/\text{H}_2\text{O}_2/\text{NH}_3$ (5:1:1) at 70°C for 1 h.

To synthesize CNTs and functionalize these with acid, we performed chemical vapor deposition in the presence of a mixture of ferrocene acting as a catalyst and toluene as a hydrocarbon source as described in literature.¹² Ali et al. have described the synthesis of NiO nanoparticles and the in situ synthesis of nanocomposite with CNTs.¹² During the NiO synthesis, CNTs (0.2%) are added into Ni(OH)_2 solution at a pH of 10.1. Owing to strong electrostatic interactions, CNTs bind with NiO nanoparticles. This thick gel-like CNT– Ni(OH)_2 solution is selectively deposited onto ITO electrode via dip coating technique. The modified substrate is dried at $\sim 110^\circ\text{C}$ for about 1 h and annealed at 450°C for about 2 h to obtain CNT–NiO composite matrix on ITO surface. Then, $15\text{ }\mu\text{L}$ of AAB solution is spread onto the CNT–NiO surface via physical adsorption followed by EDC-NHS coupling chemistry and kept for 4 h in a humid chamber (4°C). The carboxylic ($-\text{COOH}$) groups on CNT–NiO surface can undergo an amidation reaction with $-\text{NH}_2$ groups of the proteins (AAB). The covalently conjugated protein (AAB) molecule provides a strong covalent (C–N) bond formed between $-\text{COOH}$ group of CNT–NiO and $-\text{NH}_2$ group of AAB that has been confirmed via X-ray photoelectron spectrometry (XPS) and Fourier transform infrared spectroscopy (FT-IR) studies. BSA molecules are used to block the nonspecific sites of AAB functionalized CNT–NiO surface. The fabricated PDMS slab is sealed with glass substrate containing ITO electrode and BSA–AAB/CNT–NiO/ITO immunoelectrode. A

syringe pump maintains the constant flow rate ($1.0\text{ }\mu\text{L}/\text{min}$) to transport PBS and LDL solution through this chip. An Ag/AgCl wire introduced in the outlet of the microchannel worked as a reference electrode while bare ITO acted as the counter electrode. The fabricated BSA–AAB/CNT–NiO/ITO-based electrode LOC is kept at 4°C when not in use. Scheme 1 shows the fabrication of LOC and the functionalization of BSA–AAB onto CNT–NiO surface for the detection of LDL molecules.

3.3. Instrumentation. The synthesized CNTs, NiO nanoparticles, and CNT–NiO nanocomposite have been characterized using transmission electron microscopy (TEM, JEOL JEM-2000 EX) and scanning electron microscopy (SEM, Zeiss, EVO, 40). To investigate the protein (AAB) functionalization on CNT–NiO, we utilized X-ray photoelectron spectrometry (XPS, Thermo Scientific, Multilab 2000, with an alpha 110 hemispherical electron energy analyzer and an X-ray source) and Fourier transform infrared spectroscopy (FT-IR, PerkinElmer, Model 2000). The electrochemical activity of this iLOC for LDL detection has been conducted using an electrochemical workstation (Model AUT-84275) in the presence of phosphate buffer saline (50 mM, pH 7.4) containing $5\text{ mM }(\text{Fe}(\text{CN})_6)^{3-/4-}$ as a redox species.

3.4. Cell Proliferation Study. The effect of CNTs, NiO nanoparticles or CNT–NiO nanocomposite on human cell line has been studied using methyl thiazol tetrazolium (MTT) assay and bright field microscopy (Figure 1). The lung epithelial cancer cell line A549 is used as a test cell line. The A549 cells are procured from NCCS, Pune, India. The cells are maintained in a complete growth medium (10% FBS containing Roswell Park Memorial Institute; RPMI-1640) at 37°C under humidified 5% CO_2 environment. For assay, the cells are plated at 5×10^3 cell/well in 96-well tissue-culture plate and are allowed to attach for 24 h. The next day, medium on the plated cells is replaced with fresh growth medium supplemented with CNTs, NiO, or CNT–NiO nanocomposite. The nanoparticles of NiO, CNTs (1 mg/mL) or their composite comprising of NiO and CNTs in 49:1 ratio are dispersed in deionized water by continuous sonication. This suspension is kept at room temperature for 1 h to allow the nondispersed material to settle down. Prior to the addition of dispersed nanoparticles to the growth medium, the nanoparticles are again dispersed by sonication using a sonicator bath at room temperature (10 min at 40 W). The dispersed nanoparticles are

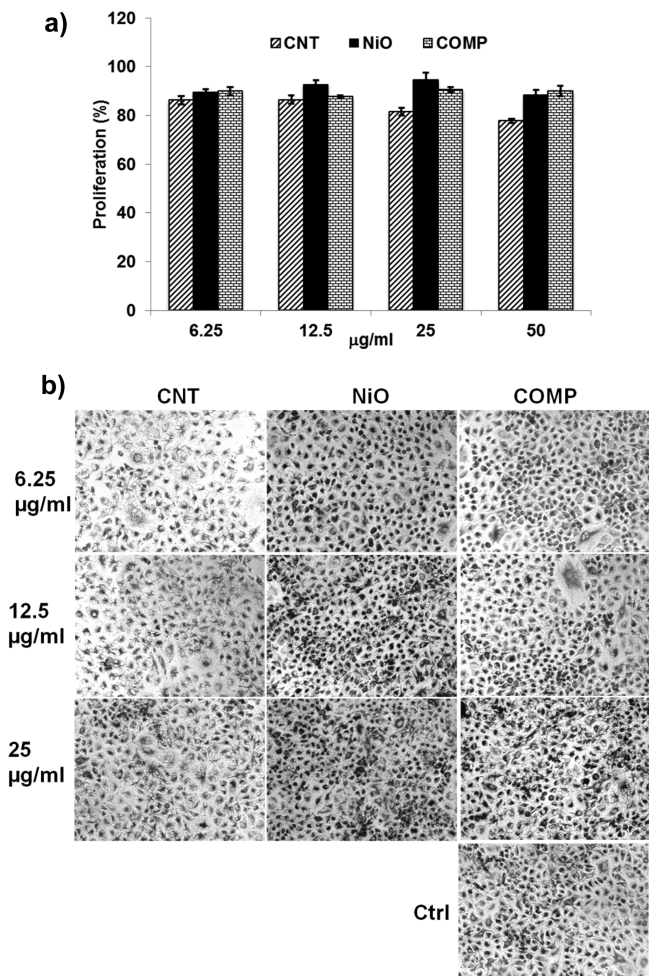


Figure 1. (a) CNT–NiO composite has reduced toxicity compared to that of CNTs alone. The A549 cells plated at 5×10^3 cells per well in 96-well tissue culture plate are exposed to growth medium containing indicated concentration of nanoparticles for 24 h. The cells are treated with MTT for 1 h and then relative reduction of MTT to formazone by cells is calculated. The relative reduction of MTT is presented as % proliferation with respect to cells not exposed to any nanoparticles (Ctrl). The error bars show average deviation. (b) CNTs exposure significantly attenuates the ability of A549 cells to reduce MTT dye to formazone as compared to NiO or CNT–NiO composite. A549 cells exposed to indicated concentration of CNTs, NiO or CNT–NiO composite (COMP) for 24 h are incubated in the presence of 1 mg/mL MTT for 1 h. The cells are imaged using Nikon eclipse microscope at 100 \times magnification.

added to the cell growth medium at a final concentration of 50, 25, 12.5, and 6.25 $\mu\text{g}/\text{mL}$.

The medium on cells is replaced with MTT containing RPMI-1640 medium after 24 h. The cells are further incubated for 1–2 h at 37 °C to allow reduction of MTT dye to formazan crystals. The cells are also observed under the inverted microscope prior to MTT addition and 1–2 h later before solubilization of cells with dimethyl sulfoxide (DMSO). The cells are solubilized in 100 μL of DMSO, followed by absorbance measurement at 540 nm. The absorbance value gives a measure of the cell proliferation. The relative proliferation is calculated with respect to cells that are not exposed to any kind of nanoparticles. In each experiment, every treatment group is replicated in three independent wells. Each experiment is repeated three times, and the average proliferation is calculated. A representative experiment is displayed where error bars represent \pm average deviation.

3. RESULTS AND DISCUSSION

3.1. Effect of Cytotoxicity. The results of MTT assay reveal that the NiO nanoparticles and CNT–NiO nanocomposite have much reduced influence on the well being of A549 cells and consequently the ability of cells to reduce MTT to formazon at all the concentrations has been investigated as compared to CNTs alone (Figure 1a). The relative % proliferation is estimated with respect to growth of the control cells (Ctrl) that are not exposed to any nanoparticles. Though the MTT assay (Figure 1a) does not show much difference among the cells exposed to CNTs, NiO nanoparticles or CNT–NiO composite up to 12.5 $\mu\text{g}/\text{mL}$ concentration, further increase in the concentration shows incremental detrimental effect in case of CNTs whereas others appear to have very little effect. The toxicity of CNTs is more evident from the pattern of formazon crystal formation in CNTs exposed cells as compared to the NiO nanoparticles or CNT–NiO composite exposed cells. The CNTs exposed cells progressively show more diffused formazon crystal formation and appearance of extracellular debris with increase in CNTs concentration while NiO nanoparticles and CNT–NiO composite exposed cells are relatively unaffected in the investigated concentration range (Figure 1b).

3.2. X-ray Photoelectron Microscopy (XPS) Studies.

The surface functionalization of AAB on CNT–NiO surface has been confirmed by XPS studies. The functional groups including $-\text{O}-\text{C}=\text{O}$, $\text{C}-\text{C}$, $\text{C}-\text{OH}$, $\text{C}-\text{O}$, $\text{C}=\text{O}$, $\text{O}-\text{C}=\text{O}$, $-\text{NH}_2$ of CNT–NiO film before and after AAB immobilization have been quantified. The XPS wide scan spectra of CNT–NiO films shows C 1s and O 1s peaks in both the curves (Figure 2i,ii). The C 1s peak position and the relative atomic percentage of various functional groups present in CNT–NiO/ITO and AAB/CNT–NiO/ITO electrodes are shown in Table S1 (Supporting Information). In curve (ii), an additional peak at 401 eV is attributed to N 1s of AAB functionalization on CNT–NiO surface. In spectra b, the prominent C–C peak observed at 284.6 eV is due to graphitic (sp^2) nature of CNTs. The additional photoemission at higher binding energies is attributed to the presence of carbon atoms bonded to other functional groups. A peak seen at 285.6 eV can be ascribed to photoelectrons emitted from carbon atoms with the sp^3 configuration. The deconvoluted peaks at 286.5 and 288.5 eV arise due to the carboxylic acid functionalization such as $-\text{C}-\text{O}$, and $-\text{O}-\text{C}=\text{O}$, respectively. These results indicate the functionalization of the CNTs by $-\text{O}-\text{C}=\text{O}$. After AAB immobilization (curve c), the peak positions of these groups are slightly changed and an additional peak at 287.7 eV appears due to amide functionalization ($-\text{N}-\text{C}=\text{O}-$ groups). The covalent surface functionalization of AAB perhaps results in shift of the binding energies. In curve (d), the peak seen at 399.0 eV is assigned to the core-level electron of N 1s. The binding energy peak at \sim 400 eV corresponds to the formation of an amide linkage on the CNTs. The binding energy peak at 400.4 eV is due to the presence of amide nitrogen ($\text{CO}-\text{NH}$) in lipid molecules and the peak at 401.5 eV is ascribed to the presence of $\equiv\text{N}$ species. The atomic concentration for $\text{O}-\text{C}=\text{O}$ is found to be as 6.2% for CNT–NiO electrode that decreases to 1.7% due to AAB incorporation. This reduced amount of the $\text{O}-\text{C}=\text{O}$ groups is perhaps utilized for binding of $-\text{NH}_2$ groups of lipid molecules.

3.3. Fourier Transform Infrared Spectroscopy (FT-IR) Studies.

The FT-IR spectrum of the various electrodes is

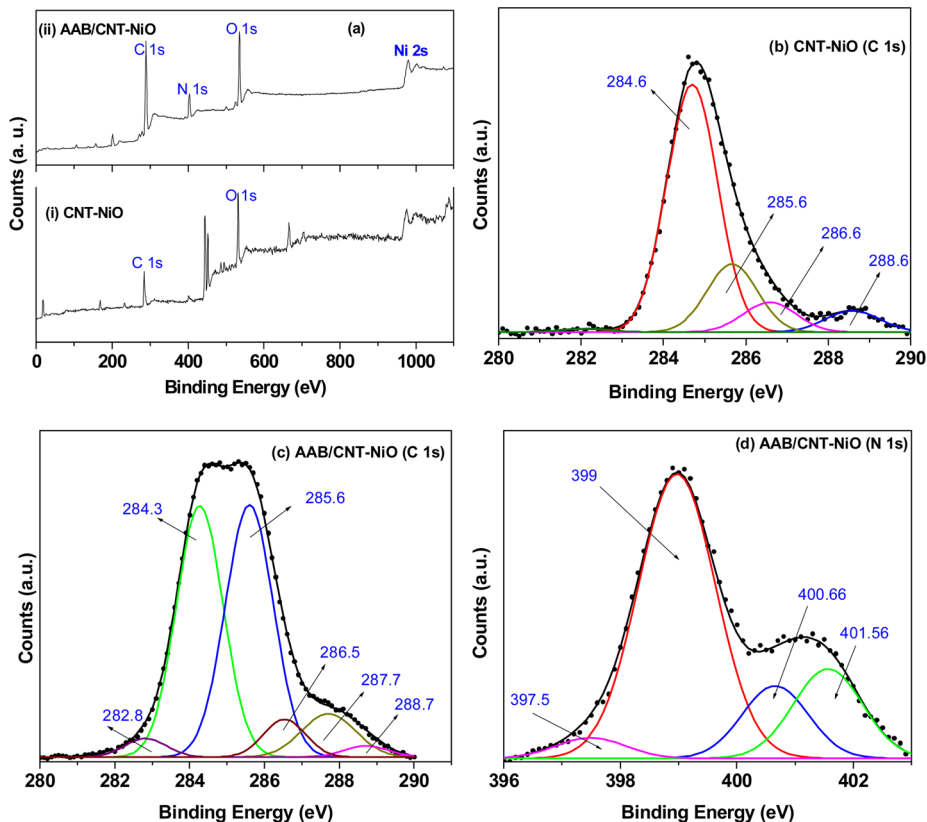


Figure 2. (a) Wide-scan XPS spectra of electrodes, (b) C 1s spectra of CNT–NiO electrode, (c) C 1s spectra of AAB functionalized CNT–NiO electrode, (d) and N 1s spectra of AAB functionalized CNT–NiO electrode.

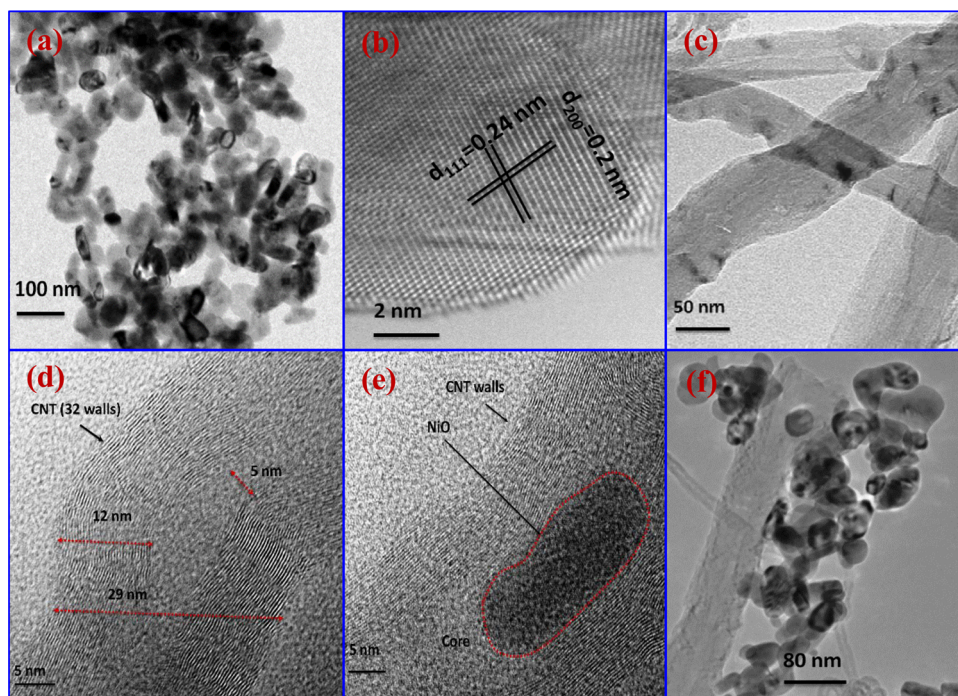


Figure 3. TEM image of (a) NiO nanoparticles, (b) lattice fringes of NiO nanoparticles (high-resolution TEM image), (c) CNTs, and (d) high-resolution image of individual CNT. (e) TEM image of elongated NiO nanoparticle with single CNT and (f) CNT modified with NiO nanoparticles.

shown in the Figure S2 (Supporting Information). The absorption peak at 503 cm^{-1} (spectra a) in the fingerprint region corresponds to Ni–O vibration band. The characteristic

absorption peaks seen at 2839 and 2917 cm^{-1} are attributed to CH stretching of COOH–CNTs. The band seen at 1562.5 cm^{-1} arises due to the C=C stretching that forms the

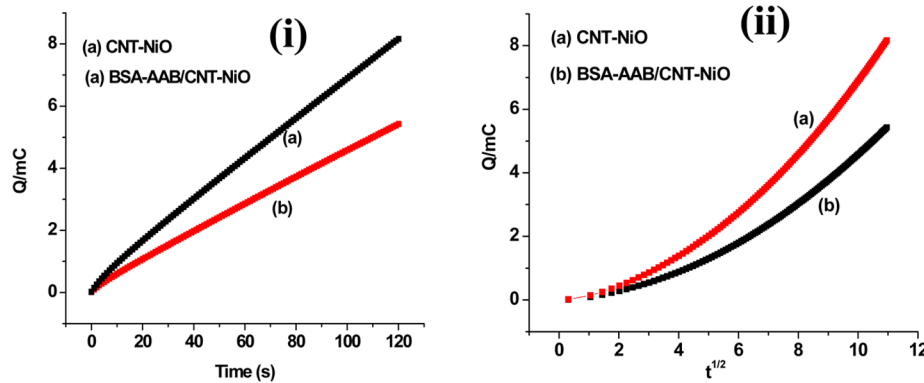


Figure 4. (i) Chronocoulometry studies of the fabricated LOC before and after protein immobilization and (ii) show the plot between charge (Q) and $t^{1/2}$.

framework of the CNT sidewall. The bands observed in the range of $2500\text{--}3000\text{ cm}^{-1}$ wavenumber result from the carboxylic acid O–H stretching. The absorption bands seen at $\sim 1000\text{--}2500\text{ cm}^{-1}$ are assigned to the O–C=O symmetric and asymmetric stretching vibrations and the C–O stretching vibration indicating CO_2 absorption on the CNT–NiO film. After immobilization of BSA–AAB onto CNT–NiO/ITO electrode surface (spectra b), the peak found at 850 cm^{-1} is assigned to the aromatic C–H bending. The peak at 1040 cm^{-1} is due to C–OH stretching vibration. The band seen at 3300 cm^{-1} is attributed to the OH stretching on the film surface. The bands seen at 1248 and 1650 cm^{-1} are due to amide III and amide I groups of BSA–AAB proteins molecules.

3.4. Morphological Studies. To observe the morphological features such as shape, size, and crystallinity of NiO, CNTs, and their composite, we have used both SEM and TEM techniques. The SEM image (Figure S3a, Supporting Information) shows an overview of the NiO nanoparticles. On addition of CNTs in NiO nanoparticles (Figure S3b, Supporting Information), it can be seen that the NiO nanoparticles are attached with majority of the carbon nanotubes (size: a few microns), which are well-dispersed on the electrode surface. These CNTs and NiO nanoparticles bind via electrostatic interactions resulting from opposite surface charges. In the case of protein (BSA and AAB) immobilized COOH-functionalized CNT–NiO electrode (Figure S3c, Supporting Information), a coating of proteins appears on the electrode surface. The dotted line indicates the separation of CNT–NiO electrode before and after proteins immobilization. The pore structure of CNT–NiO electrode is uniformly filled by BSA and AAB molecules due to strong covalent interactions between them.

The high-resolution TEM image (Figure 3a) shows that the shape of NiO is elongated and is uniformly distributed. It appears that some of the nanoparticles are spherical. The size of these NiO nanoparticles is estimated to be $<90\text{ nm}$. The highly crystalline nature of nanostructured NiO exhibits two dominant (111) and (200) planes with lattice spacing of 0.24 and 0.2 nm , respectively (Figure 3b). The micron size of CNTs with diameter $<100\text{ nm}$ can be seen in Figure 3c. The higher resolution image of CNTs, shows its inner core diameter and outer diameter (Figure 3d) as 5 and 29 nm , respectively. It can be clearly seen that the CNTs are multiwalled having 32 walls. It appears that elongated NiO nanoparticles are occupied on the core of CNTs (Figure 3e). Figure 3f exhibits that the NiO

nanoparticles are attached on the edges of CNTs on the electrode surface.

3.5. Chronocoulometry Studies. To measure the electrode surface areas, we carried out studies relating to diffusion coefficients, charges with respect to time, the mechanisms, and rate constants of chemical reactions coupled to electron transfer reactions, the chronocoulometry (CC) for various electrodes at the same step potential (1.0 V) in PBS containing ferro/ferri cyanide mediator, as shown in Figure 4i. Typical CC plots (charge-time) for CNT–NiO/ITO electrode and BSA–AAB/CNT–NiO/ITO bioelectrode (Figure 4ii) indicate charge-time dependence for linear diffusion control. It has been observed that the BSA–AAB/CNT–NiO immunoelectrode shows a fewer charge each time as compared to that of CNT–NiO/ITO electrode. The analysis of the chronocoulometric data is based on the Anson equation (eq 1) which defines the charge-time dependence for linear diffusion control:

$$Q = 2nFACD^{1/2}\pi^{1/2}t^{1/2} \quad (1)$$

where, Q represents the charge (coulombs). A plot of Q vs $t^{1/2}$ referred to as the Anson plot, where the slope (a) can be determined by the following:

$$a = 2nAFCD^{1/2}/\pi^{1/2} \quad (2)$$

where n and A represent the number of electrons transferred and the real electrochemical surface area of the electrode (cm^2), respectively. F is the Faraday constant ($96\,485\text{ coulombs/mol}$). The concentration of the mediator is denoted by C , and the diffusion coefficient of the mediator (cm^2/s) and time (s) are denoted by D and t , respectively. Therefore, the real electrochemical surface area of the electrode (A_{ec}) can be calculated from the slope in eq 3, provided the other four parameters (n , F , C , and D) are known.

$$A = a/(2nFCD^{1/2}/\pi^{1/2}) \quad (3)$$

The values of diffusion coefficient (D) of the mediator for the CNT–NiO/ITO electrode and BSA–AAB/CNT–NiO/ITO bioelectrode are found to be 6.29×10^{-9} and $2.82 \times 10^{-9}\text{ cm}^2/\text{s}$. The electrochemical active surface area (A_{ec}) is found to be as 1.9×10^{-2} and $2.0 \times 10^{-2}\text{ cm}^2$ for the CNT–NiO/ITO electrode and BSA–AAB/CNT–NiO/ITO bioelectrode, respectively. Fragkou et al. have reported the magnitude of electrochemical surface area as 0.08 cm^2 for screen printed carbon electrode (bulk electrode).³³ Fotouhi et al. have estimated the electrochemical surface for CNT–carbon paste

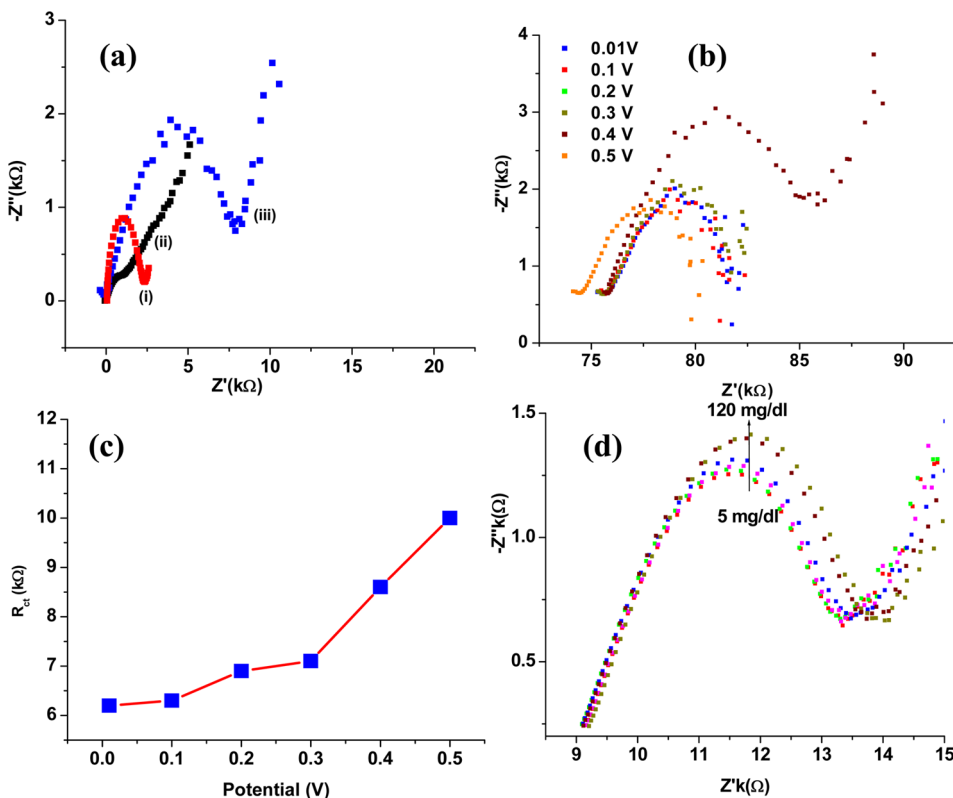


Figure 5. (a) The EIS spectra of the proposed LOC before and after BSA–AAB immobilization, (b) potential studies of the iLOC using EIS measurements, (c) plot between charge transfer resistance (R_{ct}) and potential, (d) EIS response of the iLOC (BSA–AAB/CNT–NiO) as a function of LDL concentration.

electrode as 0.9 cm^2 .³⁴ Thus, these results reveal a reasonable agreement with those reported in literature for nanostructures. Figure S4i (Supporting Information) shows potential-dependent chronocoulometric response recorded for the BSA–AAB/CNT–NiO/ITO bioelectrode at different potentials (1.0–5.0 V). It has been found that the observed charge-time response increases with increasing potential. Again, we have recorded CC curves at different flow rates ($0.01\text{--}15\text{ }\mu\text{L/min}$), as shown in Figure S4ii (Supporting Information). The Q vs $t^{1/2}$ plot for different flow rates (Figure S4iii, Supporting Information) and slope of chronocoulometric curves vs flow rates are shown in the inset of Figure S4iii (Supporting Information). At a flow rate of $1.0\text{ }\mu\text{L/min}$, the slope value is found to decrease, after which it increases to saturated value perhaps due to increased fluid velocity.³⁵

3.6. Electrochemical Impedance Spectroscopy (EIS) Studies. To investigate the nature of antigen–antibody interaction, we conducted the impedance analysis by applying a small sinusoidal AC signal as a function of frequency ($0.01\text{--}10^5\text{ Hz}$) at fixed bias potential. In the EIS measurements, the equivalent circuit model consists of the electrolyte (R_s), in series with the capacitance of the dielectric layer (C_{dl}), the charge-transfer resistance (R_{ct}), and the Warburg impedance (Z_w). In the EIS measurements (Figure 5a), the R_{ct} value of nNiO/ITO electrode (i) is found to be $2.3\text{k}\Omega$, which is higher compared to that of the CNT–NiO electrode ($2.4\text{k}\Omega$). This is due to incorporation of CNTs in the nNiO matrix, wherein CNTs play a significant role toward the improved electrochemical conductivity for redox conversation. At the electrode surface, the CNT–NiO nanocomposite acts as a mediator for electron transfer due to the decreased electron tunneling

distance from the redox probe $[\text{Fe}(\text{CN})_6]^{3-/4-}$ in bulk solution to electrode resulting in decreased R_{ct} . The C_{PE} value of CNT–NiO/ITO is found to be higher ($10.0\text{ }\mu\text{F}$) compared to that of the bioelectrode ($4.6\text{ }\mu\text{F}$) due to the BSA–AAB incorporation onto CNT–NiO/ITO surface. After the BSA–AAB immobilization, R_{ct} value of the CNT–NiO/ITO electrode (iii) increases to $11.2\text{k}\Omega$. This is attributed to the covalent interaction of proteins with the CNT–NiO molecules, which in turn impedes the ions transfer from bulk solution to electrode. The insulating characteristics of antibody and BSA on CNT–NiO/ITO transducer surface perhaps contribute toward the blocking of charge transfer through the diffusion layer. Thus, the charge transfer resistance after proteins immobilization is increased drastically. The results of cyclic voltammetry (CV) are shown in Figure S5 (Supporting Information). In CV curves, the electrochemical current for CNT–NiO electrode is found to be higher than that of nNiO electrode. CNTs provide electrochemical conduction paths for electrons generated during the redox processes resulting in enhanced electrochemical current.

The kinetic parameters such as the heterogeneous electron transfer rate constant (k_0) and the time constant (τ) of the iLOC have been evaluated to investigate the interfacial interactions of biomolecules at electrode/analyte interface. The k_0 and τ of the CNT–NiO/ITO electrode have been calculated before and after the proteins immobilization using the relations, $k_0 = RT/n^2F^2AR_{ct}C$ and $\tau = R_{ct}C_{dl} = 1/2\pi f_{max}$ respectively, where T is the temperature, R is the gas constant, n is the electron transfer constant of the redox couple, F is Faraday constant, A is the effective area of the electrode, and C is the concentration of the redox couple in the bulk solution.

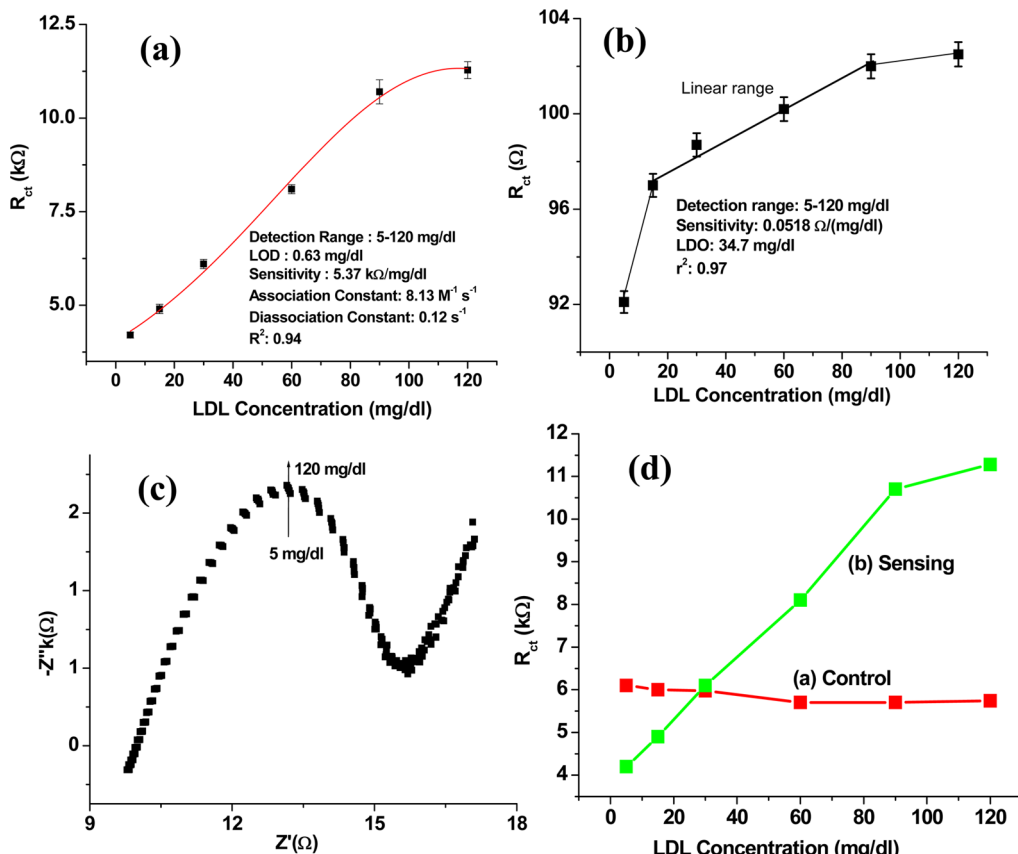


Figure 6. (a) Linear plot between the charge transfer resistance (R_{ct}) and LDL concentration of the BSA–AAB/CNT–NiO immunosensor, (b) sensor calibration plot for BSA–AAB/nNiO-based immunosensor, (c) EIS response of the iLOC by varying LDL concentration without BSA–AAB immobilization (control studies), and (d) comparison plot of LDL sensing and control experiment using CNT–NiO-based immunoelectrode.

The values of k_0 are 1.4×10^{-8} and 23.0×10^{-8} cm/s for the CNT–NiO/ITO electrode and BSA–AAB/CNT–NiO/ITO bioelectrode, respectively. The immobilization of proteins on the CNT–NiO surface leads to sluggish charge transfer rate constant resulting in the generation of low capacitance at the electrode surface. The value of τ after protein immobilization estimated to be as 5.15×10^{-2} is attributed to slow diffusion of the $[\text{Fe}(\text{CN})_6]^{3-/4-}$ ions through interface layer compared to that of the unimmobilized CNT–NiO/ITO (2.4×10^{-2}) electrode. The surface coverage (θ) can be calculated using the relation; $\theta = 1 - R_{ct(\text{electrode})}/R_{ct(\text{bioelectrode})}$, where θ is the fraction of the occupied binding sites. The $R_{ct(\text{electrode})}$ and $R_{ct(\text{bioelectrode})}$ are the surface specific charge transfer resistance of CNT–NiO/ITO electrode and BSA–AAB/CNT–NiO/ITO bioelectrode, respectively. The value of θ is estimated to be 0.8, indicating more than 80% surface coverage of the CNT–NiO/ITO electrode by BSA–AAB molecules. Considering 80% surface coverage, the number of molecules per unit area is estimated to be as 1.15×10^{-10} mol/cm 2 or 6.94×10^{13} molecules/cm 2 . Figure 5b shows EIS spectra of iLOC as a function of potential (0.01–0.5 V). It can be seen that at low potential, the EIS spectra exhibits the low charge transfer resistance. At higher potential such as 0.5 V, the iLOC shows a higher value of charge transfer resistance, as shown in Figure 5c. Thus, this potential (0.5 V) has been used to conduct the impedance response analysis.

The impedimetric response of the iLOC (BSA–AAB/CNT–NiO/ITO bioelectrode) has been measured as a function of low density lipoprotein (LDL) concentration [5–120 mg/dl]

in PBS containing $[\text{Fe}(\text{CN})_6]^{3-/4-}$ with incubation time of about 5 min (Figure 5d). The various LDL concentrations have been injected into the inlet of the microchannel by a syringe pump. The BSA molecules block the nonspecific site of AAB/CNT–NiO/ITO immunoelectrode. The variation of R_{ct} or blocking properties of the BSA–AAB/CNT–NiO/ITO bioelectrode occurs due to presence of antigen–antibody interactions at electrode/electrolyte interface. The magnitude of charge transfer resistance (R_{ct}) value increases linearly on addition of LDL concentration (Figure 6a). The presence of the insulating layer of LDL molecules on BSA–AAB/CNT–NiO/ITO bioelectrode surface inhibits diffusion of the redox species to the electrode resulting in increased diameter of EIS response. In addition, negatively charged LDL molecules may block the electron transfer of the $[\text{Fe}(\text{CN})_6]^{3-/4-}$ redox probe resulting in increased impedance. The glycine solution (0.2 M, pH 2.4) is treated for about 2 min for regeneration of the iLOC. The variation of R_{ct} with LDL concentration (5–120 mg/dl) is given by

$$R_{ct}(\Omega) = -0.66(\text{k}\Omega) + 5.3 \text{k}\Omega \text{ mg dl}^{-1} \times \text{LDL concentration} \quad (4)$$

The sensitivity of this iLOC is obtained to be as $5.3 \text{ k}\Omega/(\text{mg dl})$ with regression coefficient (r^2) as 0.94. It has been found that the impedimetric LOC exhibits improved characteristics such as low detection limit of 0.63 mg/dl (Figure 6a). It may be noted that Ali et al. have utilized protein-conjugated CdS quantum dots for estimation of LDL molecules and found

the sensitivity and detection limit of this biosensor as $98.5 \Omega (\text{mg/dL})^{-1}$ and 16.03 mg/dL , respectively.¹⁹ Thus, integration of this CNT–NiO biomaterial-based *i*LOC device provides improved sensitivity and a low detection limit for LDL detection. This is attributed to covalent functionalization of the BSA–AAB with CNT–NiO matrix on transducer surface. The values of association and dissociation constant of this *i*LOC estimated to be as $8.13 \text{ M}^{-1} \text{ s}^{-1}$ and 0.12 s^{-1} , respectively, indicate that LDL molecules have higher affinity toward this protein immobilized CNT–NiO based bioelectrode. Using reduced graphene oxide, association and dissociation constants for LDL have been found to be as $1.66 \text{ M}^{-1} \text{ s}^{-1}$ and 0.6 s^{-1} , respectively.³¹ It can be noted that the dissociation constant of this chip is higher as compared to the value reported in literature.³⁶ The higher value of the association constant reveals that CNT–NiO matrix has a good affinity toward LDL molecules. This may perhaps be due to the nanocomposite formation of CNTs with NiO enabling functionalization of the antibodies for LDL cholesterol detection with superior performance as compared to that based on reduced graphene oxide.³¹ The sensing performance using only nNiO has been carried out for detection of LDL molecules (Figure S6, Supporting Information). It has been found that the sensitivity of CNT–NiO-based immunosensor is much higher [$5.37 \text{ k}\Omega (\text{mg/dL})^{-1}$] than that based on nNiO alone [$0.0518 \Omega (\text{mg/dL})^{-1}$]. The limit of detection for nNiO-based immunosensor is higher (34.8 mg/dL) than that of CNT–NiO immunosensor (0.63 mg/dL). The lower detection limit of this CNT–NiO smart material for detection of LDL molecules may perhaps be due to available functional groups of CNTs as compared to that of nNiO immunosensor.

A control study of this proposed *i*LOC has been conducted for LDL detection using EIS method (Figure 6c). The EIS measurements have been carried out using CNT–NiO transducer chip. The observed changes in the R_{ct} values in the presence of LDL concentration are not significant as shown in Figure 6d. This may perhaps be due to the lesser affinity of LDL molecules with CNT–NiO electrode. Thus, AAB functionalized CNT–NiO immunoelectrode is highly specific, resulting in the observed changes in the impedance values.

The stability of this biochip has been evaluated for 100 days. This chip shows an excellent stability of up to 60 days with 95% response of R_{ct} value, after which the response decreases to 78%. The BSA–AAB/CNT–NiO immunoelectrode is stored at 3°C when not in use. The reproducibility of the working electrode has been investigated under similar conditions. The changes in impedance (R_{ct}) values for electrodes used in the chip are negligible, as indicated by the relative standard deviation (RSD) of 3.44%. To determine selectivity of the *i*LOC for LDL (90 mg/dL) detection, we performed EIS studies by incorporating other analytes including triglyceride (150 mg/dL), free cholesterol (150 mg/dL), and total cholesterol (150 mg/dL). We have observed a low RSD of 4.3%, indicating negligible interference with other analytes, which in turn indicates that this biochip exhibits good selectivity and stability.

4. CONCLUSIONS

An impedimetric biochip has been fabricated using functionalized CNT–NiO for LDL detection. The covalent immobilization of BSA–AAB on CNT–NiO-based LOC surface has been confirmed by XPS and FT-IR studies. The XPS studies reveal that 4.5% of O=C=O groups present in the CNT–NiO electrode are utilized to bind with amine groups of BSA–AAB

molecules. This covalent immobilization of specific protein molecules results in higher sensitivity and a low detection limit for LDL detection. We have evaluated the binding kinetics of antigen–antibody interaction in the sensor surface. In addition, this LOC is found to be highly selective, has a good stability and a wide detection range of $5\text{--}120 \text{ mg/dL}$ within the physiological range of LDL. The cytotoxicity studies of CNTs, NiO, and CNT–NiO composite have been performed in the presence of human lung epithelial cancer cells using MTT assay. The electron microscopic studies of the CNT–NiO composite in this LOC shows integration of NiO nanoparticles with COOH-functionalized CNTs. The cytotoxicity test indicates that a CNT–NiO composite-based biochip is a better and safer choice for this application. The CNT–NiO composite provides a biocompatible and favorable environment due to high surface-to-volume ratio resulting in enhanced loading capacity of AAB. The application of CNT–NiO composite not only improves the electrochemical impedance characteristics for LDL detection but results in enhanced loading capacity of proteins. The high sensitivity combined with specificity of LDL-AAB binding toward LDL detection using CNT–NiO is an interesting platform that can be used to detect other biomolecules. This *i*LOC requires a minute amount of sample, indicating that this miniaturized compact device has high potential for application as point-of-care diagnostics.

■ ASSOCIATED CONTENT

Supporting Information

Photolithographic process for fabrication of patterned ITO electrode, FT-IR studies, SEM studies, electrochemical studies (chronocoulometric, cyclic voltammetry, and impedance), and a Table containing results of XPS measurements. This material is available free of charge via the Internet at <http://pubs.acs.org>.

■ AUTHOR INFORMATION

Corresponding Author

*E-mail: bansi.malhotra@gmail.com. Tel.: 91 11 27871043, ext. 1609. Lab Tel.: 91 11 27294668. Fax: 91-11-27871023.

Notes

The authors declare no competing financial interest.

■ ACKNOWLEDGMENTS

We thank Director NPL, New Delhi, India, for the facilities. M.A.A. is thankful to CSIR, India, for the award of Senior Research Fellowships. The financial support received from Department of Science and Technology, India (Grant No. DST/TSG/ME/2008/18), and Indian Council of Medical Research, India (Grant No. ICMR/5/3/8/91/GM/2010-RHN), is gratefully acknowledged.

■ REFERENCES

- (1) Yang, W.; Ratinac, K. R.; Ringer, S. P.; Thordarson, P.; Gooding, J. J.; Braet, F. Carbon Nanomaterials in Biosensors: Should You Use Nanotubes or Graphene? *Angew. Chem., Int. Ed.* **2010**, *49*, 2114–2138.
- (2) Medina-Sánchez, M.; Miserere, S.; Merkoçi, A. Nanomaterials and Lab-on-a-Chip Technologies. *Lab Chip* **2012**, *12*, 1932–1943.
- (3) Wang, Y.-F.; Liu, G.-Y.; Sun, L.-D.; Xiao, J.-W.; Zhou, J.-C.; Yan, C.-H. Nd³⁺-Sensitized Upconversion Nanophosphors: Efficient in Vivo Bioimaging Probes with Minimized Heating Effect. *ACS Nano* **2013**, *7*, 7200–7206.
- (4) Crevillén, A. G.; Pumera, M.; González, M. C.; Escarpa, A. Towards Lab-on-a-Chip Approaches in Real Analytical Domains based

- on Microfluidic Chips/Electrochemical Multi-Walled Carbon Nanotube Platforms. *Lab Chip* **2009**, *9*, 346–353.
- (5) Craighead, H. Future Lab-on-a-Chip Technologies for Interrogating Individual Molecules. *Nature* **2006**, *442*, 387–393.
- (6) Misewich, J.; Martel, R.; Avouris, P.; Tsang, J.; Heinze, S.; Tersoff, J. Electrically Induced Optical Emission from a Carbon Nanotube FET. *Science* **2003**, *300*, 783–786.
- (7) Sharf, T.; Kevek, J. W.; DeBorde, T.; Wardini, J. L.; Minot, E. D. Origins of Charge Noise in Carbon Nanotube Field-Effect Transistor Biosensors. *Nano Lett.* **2012**, *12*, 6380–6384.
- (8) Choi, J. H.; Nguyen, F. T.; Barone, P. W.; Heller, D. A.; Moll, A. E.; Patel, D.; Boppart, S. A.; Strano, M. S. Multimodal Biomedical Imaging with Asymmetric Single-Walled Carbon Nanotube/Iron Oxide Nanoparticle Complexes. *Nano Lett.* **2007**, *7*, 861–867.
- (9) Napier, M. E.; Hull, D. O.; Thorp, H. H. Electrocatalytic Oxidation of DNA-Wrapped Carbon Nanotubes. *J. Am. Chem. Soc.* **2005**, *127*, 11952–11953.
- (10) Lin, Y.; Taylor, S.; Li, H.; Fernando, K. S.; Qu, L.; Wang, W.; Gu, L.; Zhou, B.; Sun, Y.-P. Advances toward Bioapplications of Carbon Nanotubes. *J. Mater. Chem.* **2004**, *14*, 527–541.
- (11) Periasamy, A. P.; Yang, S.; Chen, S.-M. Preparation and Characterization of Bismuth Oxide Nanoparticles-Multiwalled Carbon Nanotube Composite for the Development of Horseradish Peroxidase based H_2O_2 Biosensor. *Talanta* **2011**, *87*, 15–23.
- (12) Ali, M. A.; Srivastava, S.; Solanki, P. R.; Reddy, V.; Agrawal, V. V.; Kim, C.; John, R.; Malhotra, B. D. Highly Efficient Bienzyme Functionalized Nanocomposite-based Microfluidics Biosensor Platform for Biomedical Application. *Sci. Rep.* **2013**, *3*, 2661.
- (13) Salimi, A.; Sharifi, E.; Noorbakhsh, A.; Soltanian, S. Immobilization of Glucose Oxidase on Electrodeposited Nickel Oxide Nanoparticles: Direct Electron Transfer and Electrocatalytic Activity. *Biosens. Bioelectron.* **2007**, *22*, 3146–3153.
- (14) Lewis, J. A. Colloidal Processing of Ceramics. *J. Am. Ceram. Soc.* **2000**, *83*, 2341–2359.
- (15) Daw, R.; Finkelstein, J. Insight: Lab on a Chip. *Nature* **2006**, *442*, 367–418.
- (16) Stone, H. A.; Stroock, A. D.; Ajdari, A. Engineering Flows in Small Devices: Microfluidics toward a Lab-on-a-Chip. *Annu. Rev. Fluid Mech.* **2004**, *36*, 381–411.
- (17) Ruan, C.; Yang, L.; Li, Y. Immunobiosensor Chips for Detection of *Escherichia coli* O157:H7 using Electrochemical Impedance Spectroscopy. *Anal. Chem.* **2002**, *74*, 4814–4820.
- (18) Carlborg, C. F.; Gylfason, K. B.; Kaźmierczak, A.; Dortu, F.; Polo, M. B.; Catala, A. M.; Kresbach, G.; Sohlström, H.; Moh, T.; Vivien, L. A Packaged Optical Slot-Waveguide Ring Resonator Sensor Array for Multiplex Label-free Assays in Labs-on-Chips. *Lab Chip* **2010**, *10*, 281–290.
- (19) Ali, M. A.; Srivastava, S.; Pandey, M. K.; Agrawal, V. V.; John, R.; Malhotra, B. D. Protein-Conjugated Quantum Dots Interface: Binding Kinetics and Label-Free Lipid Detection. *Anal. Chem.* **2014**, *86*, 1710–1718.
- (20) Matharu, Z.; Bandodkar, A. J.; Suman, G.; Solanki, P. R.; Ekanayake, E. M.; Kaneto, K.; Gupta, V.; Malhotra, B. Low Density Lipoprotein Detection based on Antibody Immobilized Self-Assembled Monolayer: Investigations of Kinetic and Thermodynamic Properties. *J. Phys. Chem. B* **2009**, *113*, 14405–14412.
- (21) Lacerda, L.; Bianco, A.; Prato, M.; Kostarelos, K. Carbon Nanotubes as Nanomedicines: from Toxicology to Pharmacology. *Adv. Drug Delivery Rev.* **2006**, *58*, 1460–1470.
- (22) Kostarelos, K. The Long and Short of Carbon Nanotube Toxicity. *Nat. Biotechnol.* **2008**, *26*, 774–776.
- (23) Al Faraj, A.; Cieslar, K.; Lacroix, G.; Gaillard, S.; Canet-Soulas, E.; Crémillieux, Y. In Vivo Imaging of Carbon Nanotube Biodistribution using Magnetic Resonance Imaging. *Nano Lett.* **2009**, *9*, 1023–1027.
- (24) Jia, G.; Wang, H.; Yan, L.; Wang, X.; Pei, R.; Yan, T.; Zhao, Y.; Guo, X. Cytotoxicity of Carbon Nanomaterials: Single-Wall Nanotube, Multi-Wall Nanotube, and Fullerene. *Environ. Sci. Technol.* **2005**, *39*, 1378–1383.
- (25) Magrez, A.; Kasas, S.; Salicio, V.; Pasquier, N.; Seo, J. W.; Celio, M.; Catsicas, S.; Schwaller, B.; Forró, L. Cellular Toxicity of Carbon-based Nanomaterials. *Nano Lett.* **2006**, *6*, 1121–1125.
- (26) Zhang, Y.; Ali, S. F.; Dervishi, E.; Xu, Y.; Li, Z.; Casciano, D.; Biris, A. S. Cytotoxicity Effects of Graphene and Single-Wall Carbon Nanotubes in Neural Phaeochromocytoma-Derived PC12 Cells. *ACS Nano* **2010**, *4*, 3181–3186.
- (27) Ryoo, S.-R.; Kim, Y.-K.; Kim, M.-H.; Min, D.-H. Behaviors of NIH-3T3 Fibroblasts on Graphene/Carbon Nanotubes: Proliferation, Focal Adhesion, and Gene Transfection Studies. *ACS Nano* **2010**, *4*, 6587–6598.
- (28) Davoren, M.; Herzog, E.; Casey, A.; Cottineau, B.; Chambers, G.; Byrne, H. J.; Lyng, F. M. In Vitro Toxicity Evaluation of Single Walled Carbon Nanotubes on Human A549 Lung Cells. *Toxicol. In Vitro* **2007**, *21*, 438–448.
- (29) Mooney, E.; Dockery, P.; Greiser, U.; Murphy, M.; Barron, V. Carbon Nanotubes and Mesenchymal Stem Cells: Biocompatibility, Proliferation and Differentiation. *Nano Lett.* **2008**, *8*, 2137–2143.
- (30) Lopes-Virella, M. F.; Stone, P.; Ellis, S.; Colwell, J. Cholesterol Determination in High-Density Lipoproteins Separated by Three Different Methods. *Clin. Chem.* **1977**, *23*, 882–884.
- (31) Ali, M. A.; Kamil Reza, K.; Srivastava, S.; Agrawal, V. V.; John, R.; Malhotra, B. D. Lipid–Lipid Interactions in Aminated Reduced Graphene Oxide Interface for Biosensing Application. *Langmuir* **2014**, *30*, 4192–4201.
- (32) Ali, M. A.; Solanki, P. R.; Patel, M. K.; Dhayani, H.; Agrawal, V. V.; John, R.; Malhotra, B. D. A Highly Efficient Microfluidic Nano Biochip based on Nanostructured Nickel Oxide. *Nanoscale* **2013**, *5*, 2883–2891.
- (33) Fragkou, V.; Ge, Y.; Steiner, G.; Freeman, D.; Bartetzko, N.; Turner, A. P. Determination of the Real Surface Area of a Screen-Printed Electrode by Chronocoulometry. *Int. J. Electrochem. Sci.* **2012**, *7*, 6214–6220.
- (34) Fotouhi, L.; Fatollahzadeh, M.; Heravi, M. M. Electrochemical Behavior and Voltammetric Determination of Sulfaguanidine at a Glassy Carbon Electrode Modified with a Multi-Walled Carbon Nanotube. *Int. J. Electrochem. Sci.* **2012**, *7*, 3919–3928.
- (35) Mulchandani, P.; Chen, W.; Mulchandani, A. Flow Injection Amperometric Enzyme Biosensor for Direct Determination of Organophosphate Nerve Agents. *Environ. Sci. Technol.* **2001**, *35*, 2562–2565.
- (36) Matharu, Z.; Arya, S. K.; Sumana, G.; Gupta, V.; Malhotra, B. Self-Assembled Monolayer for Low Density Lipoprotein Detection. *J. Mol. Recognit.* **2008**, *21*, 419–424.